1-1-2018

Tetragonality of bcc Phases in a Transformation-Induced Plasticity Steel

Zhiping Xiong
University of Wollongong, zx868@uowmail.edu.au

David R. G Mitchell
University of Wollongong, dmitchel@uow.edu.au

Ahmed A. Saleh
University of Wollongong, asaleh@uow.edu.au

Elena V. Pereloma
University of Wollongong, elenap@uow.edu.au

Tetragonality of bcc Phases in a Transformation-Induced Plasticity Steel

Abstract

In a low-alloyed multi-phase transformation-induced plasticity steel, solute carbon content in polygonal ferrite, bainitic ferrite, and martensite was characterized using site-specific atom probe tomography. Selected area diffraction patterns were obtained using transmission electron microscopy, and the geometric distortion thereof was determined. The results showed that the lattice distortion increased in a sequence of polygonal ferrite, lath-like bainitic ferrite, and martensite. This increasing distortion corresponded to an increase in carbon content of the phase.

Publication Details

Xiong, Z., Mitchell, D. R.G., Saleh, A. A. & Pereloma, E. V. (2018). Tetragonality of bcc Phases in a Transformation-Induced Plasticity Steel. Metallurgical and Materials Transactions A: Physical Metallurgy and Materials Science, 49 (12), 5925-5929.

Tetragonality of bcc phases in a transformation-induced plasticity steel

ZHIPING XIONG[1], DAVID R.G. MITCHELL[2], AHMED A. SALEH[1], and ELENA V. PERELOMA[1, 2, *]

[1]School of Mechanical, Materials, Mechatronic and Biomedical Engineering, University of Wollongong, Wollongong, NSW, 2522, Australia
[2]Electron Microscopy Centre, University of Wollongong, Wollongong, NSW, 2519, Australia
*Correspondence author email address: elenap@uow.edu.au.

Abstract: In a low-alloyed multi-phase transformation-induced plasticity steel, solute carbon content in polygonal ferrite, bainitic ferrite and martensite was characterized using site-specific atom probe tomography. Selected area diffraction patterns were obtained using transmission electron microscopy (TEM), and the geometric distortion thereof was determined. The results showed that the lattice distortion increased in a sequence of polygonal ferrite, lath-like bainitic ferrite and martensite. This increasing distortion corresponded to an increase in carbon content of the phase.

In steels, during cooling from the austenitization temperature, polygonal ferrite, bainite and martensite can form sequentially. It is well known that polygonal ferrite forms via a diffusional mechanism at a slow cooling rate from the austenitization temperature, according to the equilibrium Fe-C phase diagram, leading to a body-centered cubic (bcc) structure [1]. Under rapid cooling conditions from the austenitization temperature, martensite is formed. This occurs via a displacive mechanism, in which all atoms move some fractions of an interatomic distance, resulting in a body-centered tetragonal structure in medium-high carbon steels [2]. At intermediate cooling rates, bainite forms in a temperature range between those at which polygonal ferrite and martensite form. This has led to a decades-old debate as to whether or not the bainite formation mechanism is diffusion-controlled [3] or displacive-controlled [4].

Recently, the carbon content in defect-free lath bainitic ferrite (BF) has been measured using atom probe tomography (APT) and has been found to be higher than para-equilibrium [5-9]. This demonstrates the assumption that this phase contains excess carbon due to trapping of carbon at defects is not correct [5]. Tetragonality (distortion) of the bcc lattice occurs commonly in high carbon martensite where an ordered structure of solute carbon atoms results from the shear mechanism of phase transformation manifesting in carbon super-saturation compared to the equilibrium state of ferrite [10-14]. It was also suggested to be the reason for the observed carbon

super-saturation in BF laths [15]. In-situ synchrotron, neutron and X-ray diffraction (XRD) obtained from a range of different steels after suitable ageing (as listed in Table 1) showed that the resulting BF laths had tetragonality. In addition, a decrease in tetragonality of BF laths occurred with increasing holding time of bainitic steels as a result of the carbon diffusing from the BF lath to the neighboring austenite [6, 17].

Table 1. The heat treatment for different steels.

Chemical compositions, wt. %	Heat treatment for bainitic transformation	Reference
Fe-0.84C-2.26Mn-1.78Si-1.55Co-1.47Cr-0.25Mo-0.11V-0.11Cu	200 °C for 10 days	[16]
Fe-0.7C-1.4Si-1.3Mn-1.0Cr-0.2Mo-0.1Ni	220 °C for 1 day	[6]
Fe-0.8C-1.6Si-2.0Mn-1.0Cr-0.2Mo-4.0Co-1.7Al	250 °C for 0.5 day	[6]
Fe-1.04C-3.89Si-1.97Mn-0.24Mo-1.43Al	300 °C for 1 day	[17]

The tetragonality of BF laths in bainitic steels has received significant attention [6, 8, 16, 17]. However, limited data are available for bcc phases in multi-phase steels. In addition, it is very important that advanced technologies should be employed in tetragonality characterization as new scientific information could be found because of improved accuracy. The present paper studies the tetragonality in bcc phases (polygonal ferrite, BF laths and martensite) in a low-alloyed multi-phase transformation-induced plasticity (TRIP) steel using high-resolution transmission electron microscopy (TEM). The relationship between tetragonality and solute carbon content fits very well to the recently published data using high-resolution XRD.

A low-alloyed multi-phase TRIP steel (Fe-0.17C-1.61Mn-1.52Si-0.20Cr, wt. %) was produced using a laboratory simulated strip casting process, which included an isothermal holding at 400 °C for 900 s [18]. The microstructure consisted of 55% polygonal ferrite, 4.5 % retained austenite (RA), carbide-free bainite (BF, granular bainite (GB)), and small amounts of martensite and Widmanstätten ferrite (WF) as shown in a representative electron backscattering diffraction (EBSD) map in Figure 1. Examples of martensite and WF were reported in previous studies [7, 18].

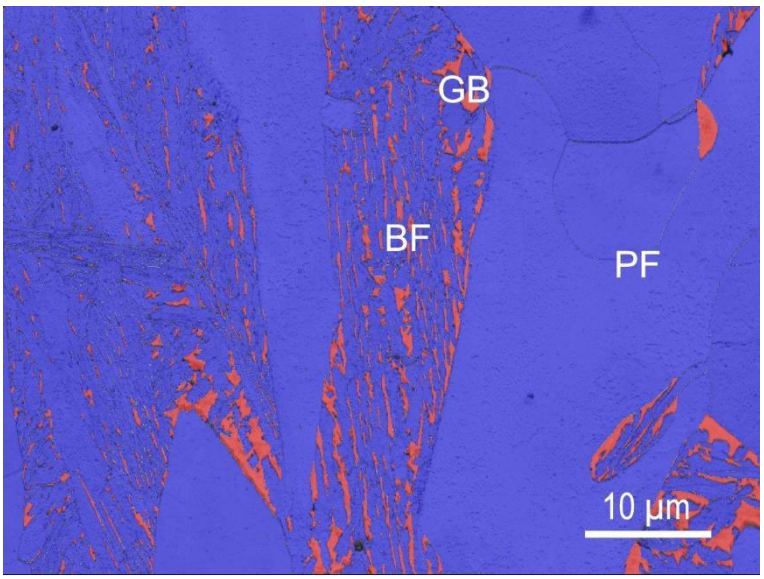

Fig.1—A representative EBSD phase map showing BCC phases in blue and FCC austenite in red. *BF* is bainitic ferrite, *GB* is granular bainite and *PF* is polygonal ferrite.

Site-specific tips for APT were micro-machined based on EBSD maps. APT experiments were carried out using a local electrode atom probe (LEAP 4000 HR, Cameca Instruments). The details have been published in Ref. [7]. It is emphasized here that the chemical compositions of the BCC phases were calculated from the volumes containing no clusters, precipitates or solute segregation.

Foils for TEM characterization were prepared using focused ion beam (FIB) milled (Helios NanoLab G3 CX dual-beam, FEI) lift-outs with the help of EBSD phase maps to identify suitable lift-out locations. Foils were characterized using a JEOL ARM 200F instrument operated at 200 kV. Selected area diffraction (SAD) patterns were acquired at a camera length of 30 cm. Camera lengths had been calibrated previously using a polycrystalline gold reference specimen. Electron diffraction patterns are subject to an intrinsic distortion, as a result of lens distortions, mechanical misalignments and aberrations. A typical manufacturer's installation is that this distortion should be less than 1%. The correction of this distortion (to reveal the true extent of any tetragonality) was carried out as described below.

A polycrystalline gold on carbon specimen provided ring diffraction patterns (Figure 2(a)). Ellipse fitting analysis (EFA) was used to measure the distortion [19]. This showed an elliptical distortion of 0.91±0.26% (distortion is defined as (1-(minor axis/major axis))×100%) at an angle of 160 degrees with respect to the horizontal, ie. a vector pointing to approximately 10 o'clock would be parallel to the major axis of the ellipse. The elliptical distortion was corrected by warping the pattern, leading to a decrease in elliptical distortion to 0.26±0.03%. For verification, single crystal patterns of silicon with the beam parallel to the [001] direction (Figure 2(b)) were obtained under identical conditions to those used for polycrystalline gold. A Si <400> vector

lay close to the major axis of distortion. The measured distortion in the as-recorded pattern was obtained by comparing the length of this Si <400> vector with its orthogonal counterpart. This gave a value of 0.73%. The Si [001] pattern (Figure 2(b)) was warped using the distortion parameters obtained from the gold pattern (Figure 2(a)), and the overall distortion was reduced to 0.36% (Figure 2(c)). Thus, this was generally consistent with that measured in polycrystalline gold, which demonstrated the reliability of this correction method.

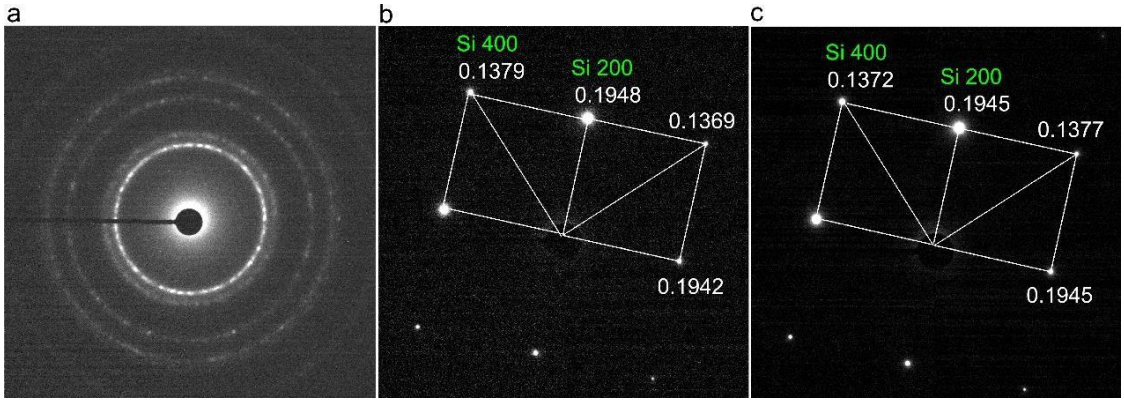

Fig. 2—(a) Selected area diffraction pattern from polycrystalline gold; (b) uncorrected and (c) corrected selected area diffraction patterns from single crystal of silicon with the beam parallel to [001]. The values are measured lattice spacing in Å.

As an example, Figure 3(a) shows a carbon atom map from a volume which included enriched (carbide) and depleted (BF lath) regions, while Figure 3(b-d) show homogeneous distribution of manganese, silicon and chromium. Chemical gradients (Figure 3(e)) were revealed using proximity histograms at iso-concentration surfaces of 3.0 at. % C, namely the proximate interface between BF lath and carbide. As expected, carbon and manganese were enriched while silicon was depleted in the carbide. The chemical composition of this BF lath was calculated in the homogeneous region (cylinder in Figure 3(a)) without any visible segregation and clustering. Similar measurements were undertaken to determine the compositions of polygonal ferrite, BF lath and martensite from numerous locations. Here, the statistic carbon content for each phase is listed in Table 2, which shows an increased sequence of carbon content from PF to BF lath to martensite.

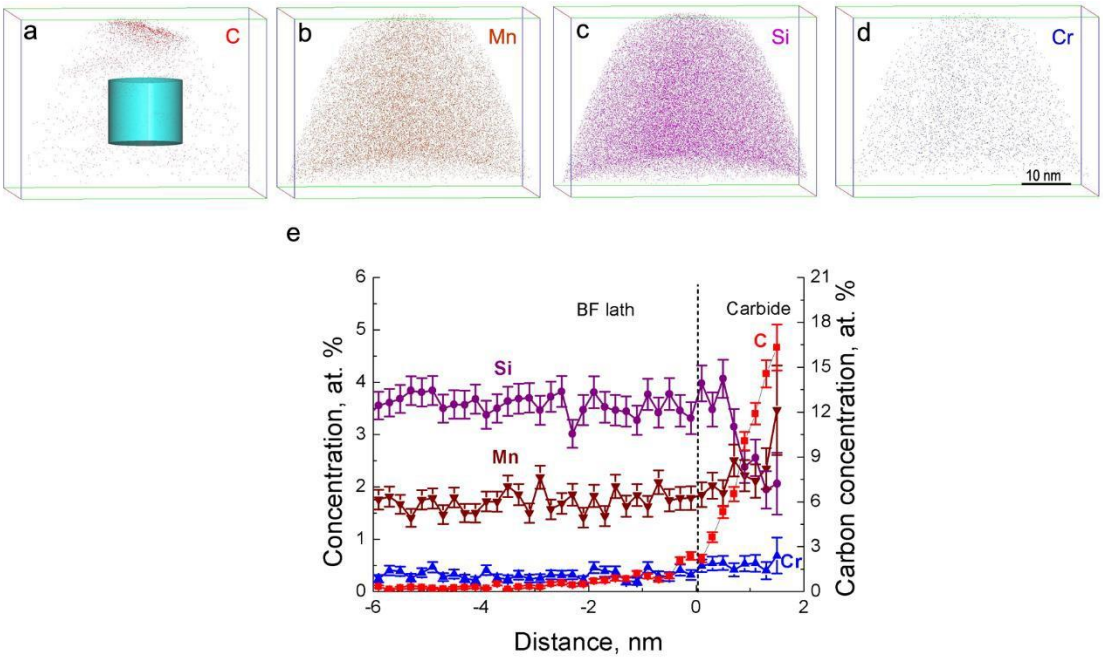

Fig. 3—Atom maps of (a) carbon (the blue cylinder is a volume which shows no segregation or clustering and from which the composition was determined), (b) manganese, (c) silicon and (d) chromium; (e) proximity histogram across the interface between a BF lath and carbide at the iso-concentration surface of 3.0 at. % C (the left y-axis corresponds to Si, Mn and Cr).

Table 2. Summary of carbon content and corrected lattice distortion.

	Carbon content, at. % (wt. %)*	Corrected distortion, %**
Polygonal ferrite	0.027±0.002 (0.0063±0.0005)	0.08±0.07
Bainitic ferrite lath	0.32±0.16 (0.075±0.038)	0.83±0.14
Martensite	2.7±0.5 (0.61±0.12)	1.16

* determined from APT data; ** determined from SAD patterns.

Figure 4(a) and (c) show an example of a BF lath and its distortion-corrected SAD pattern, respectively; while Figure 4(b) shows martensite between WF and a bainitic packet, and its corrected SAD pattern was shown in Figure 4(d). The measured lattice distortion (according to *section 2.2*) is summarized in Table II. The polygonal ferrite had the lowest distortion of 0.08±0.07 %, which is effectively zero. After distortion correction of the calibration polycrystalline gold pattern, its residual distortion was 0.26±0.03%. Thus, a distortion of about 0.3% is probably the real limit of precision for this technique. The BF lath showed statistically significant lattice distortion (0.83±0.14 %) while the martensite showed the greatest degree of distortion (1.16 %). Garcia-Mateo *et al.* [6] used high-resolution TEM to measure lattice spacings in a Fe-1.0C-1.5Si-1.9Mn-1.3Cr-0.26Mo-0.1V (wt. %) bainitic steel isothermal held at 200 °C for 6 days. They found that along [010] and [001] directions the spacings were 0.286 and 0.289 nm, respectively, corresponding to a 1.05 % distortion. This is

slightly higher than 0.83 % measured in the present material, although their BF lath had a higher carbon content (up to ~ 0.55 at. %) compared with 0.32±0.16 at. % in the present work. A significant difference in the distortion between the BF lath (0.83 %) and martensite (1.16 %) was found here. Although dislocations may influence this distortion, measurements of dislocation densities of BF lath ($10^{14} \sim 10^{15}$ m^{-2}) [7, 20] and martensite ($10^{14} \sim 10^{15}$ m^{-2}) [21] in similar steels to those studied here were very similar. In addition, the substitutional alloying elements were comparable between BF lath and martensite (such as c.f. 1.85±0.11 vs 1.86±0.14 at. % Mn) due to their quick formations at low temperatures. These suggest that the observed difference in lattice distortion is a structural effect.

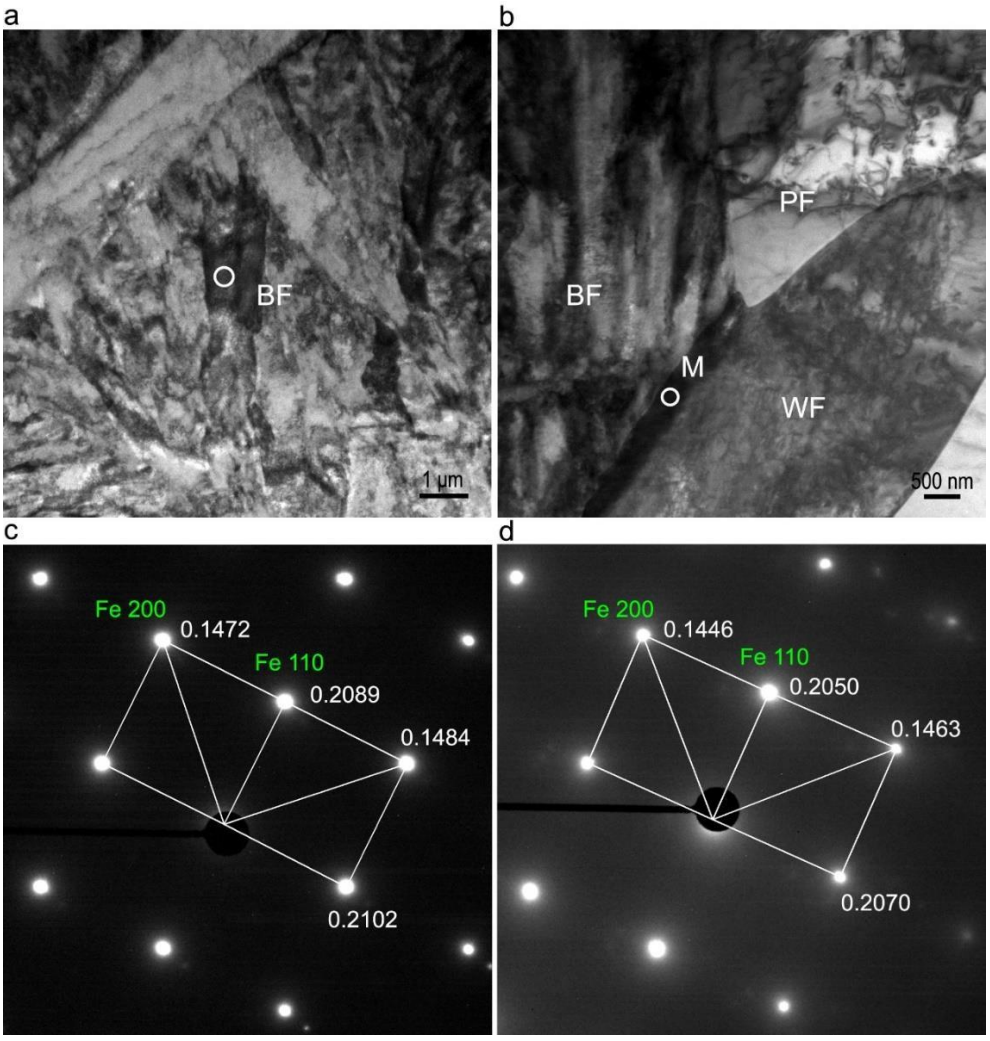

Fig. 4—Bright field images of (a) BF lath and (b) martensite with corresponding distortion-corrected SAD patterns (c) and (d) from the regions circled in (a) and (b) respectively. The zone axis of (c, d) is [011]α. The numbers in (c, d) are lattice spacings in Å. *BF* is bainitic ferrite, *PF* is polygonal ferrite, *WF* is Widmanstätten ferrite and *M* is martensite.

Polygonal ferrite forms in a diffusional process, and has a very low carbon solubility

(0.027±0.002 at. %). The measured lattice distortion of this BCC lattice (0.08±0.07%) was effectively zero. Both the BF lath and martensite formed in a low temperature regime, resulting in a high carbon content of 0.32±0.16 and 2.7±0.5 at. % (Table II), respectively. The large distortion (tetragonality) of these two phases (BF lath = 0.83±0.14 % and martensite = 1.16 %) determined from SAD patterns arises from the high carbon concentrations – the degree of tetragonality increasing with carbon concentration [5, 17]. Due to low temperature transformation, the Bain strain [22] transfers carbon atoms in one octahedral interstice per iron atom in the face-centered cubic lattice to interstices in the BCC lattice of ferrite. Carbon would preferentially occupy just one of the three sub-lattices of octahedral sites rather than tetrahedral sites in the BCC lattice due to smaller solution energy in the former [15]. This phenomenon causes cube edge distortion and in turn tetragonality, due to the octahedral site being limited to accommodating only those atoms which are smaller than carbon. XRD analysis also demonstrated the tetragonality in BF lath and martensite, and that the degree of tetragonality varies with carbon content in the BF lath [6, 16, 18]. The linear relationship between the c/a ratio and carbon content has been established based on XRD data for martensite [13, 23, 24].

Figure 5 shows the evolution of distortion with carbon content. The data for Fe-C martensite retrieved from Refs. [13, 23, 24] was also included, where distortion was calculated as (c-a)/a. The data from Refs. [13, 23] collected in 1950-1970s shows a larger distortion than the data from Ref. [24] published in 2017. This difference is probably ascribed to the improvement of X-ray diffractometer instrumentation and utilization of Rietveld refinement with related software. It means that advanced technologies are important in tetragonality characterization because they can provide excellent accuracy and in turn maybe offer new information and further reconsideration on this old topic. As shown by dashed line, the measured distortion in the present study has a reasonable fit with the newest data in Ref. [24]. The fluctuation along this dashed line is probably due to the experimental error. In addition, the variation between the data in the literature and the current work could be related to the difference in investigated materials compositions and processing. Alloying elements interactions with carbon could have occurred after completion of BF formation during subsequent holding at 400°C. Different alloying elements have different effects on lattice spacing. It has been reported that carbide-forming elements remove carbon atoms from their ordered positions and reduce the martensite lattice tetragonality, while non-carbide forming substitutional elements increase it due to their effect on carbon activity in iron [25].

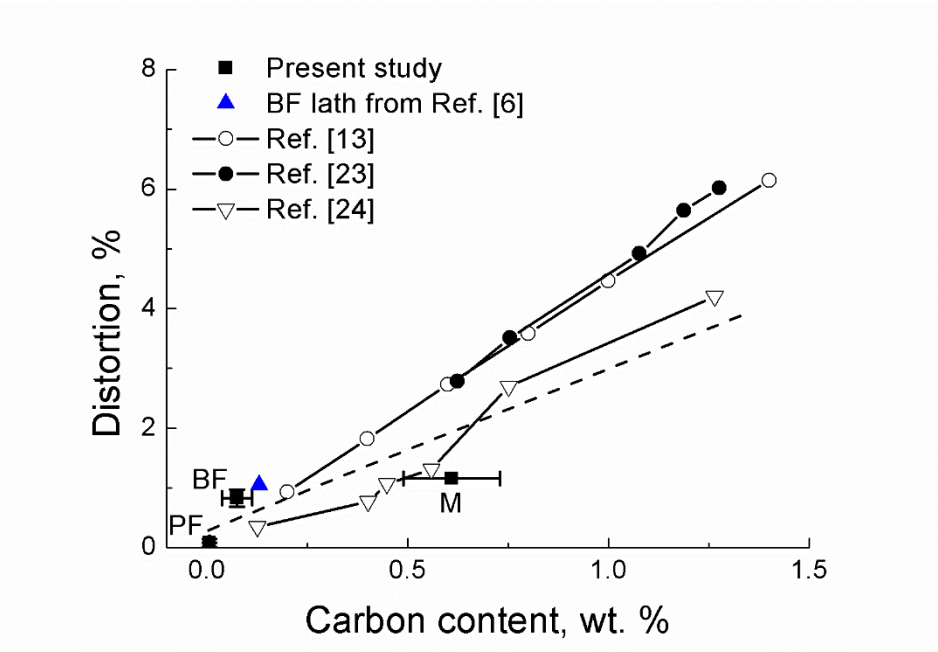

Fig. 5—The evolution of distortion in SAD pattern with carbon content. Solid lines are deduced from the XRD data for martensite [13, 23, 24]. *PF* is polygonal ferrite, *BF* is bainitic ferrite lath and *M* is martensite.

To summarise, site-specific APT and TEM/electron diffraction investigations on a low-alloyed multiphase TRIP steel directly showed an increase in carbon content (measured from a defect-free volume) and indirectly demonstrated an increase in tetragonality, in a sequence of polygonal ferrite, BF lath and martensite. Similar to martensite, the excess of carbon in the BF results in lattice tetragonality. Although these data showed somewhat deviation from the linear relationship between tetragonality and carbon content determined for martensite in 1950-1970s, they fitted well to the data recently obtained using high-resolution XRD, indicating the importance of advanced technologies for future research and reconsideration in tetragonality.

Acknowledgements: This project was supported and the JEOL JEMARM200F was funded by the Australian Research Council (DP130101887 and LE120100104, respectively). The authors thank R.K.W. Marceau, University of Deakin, for atom probe data acqusition.

References:

1. H.K.D.H. Bhadeshia: *Progr. Mater. Sci.*, 1985, vol. 29, pp. 321-386.
2. J. Christian: *Mater. Trans. JIM*, 1992, vol. 33, pp. 208-214.
3. M. Hillert, L. Höglund, and J. Ågren: *Metall. Mater. Trans. A*, 2004, vol. 35, pp. 3693-3700.
4. H. Bhadeshia and D. Edmonds: *Acta Metall.*, 1980, vol. 28, pp. 1265-1273.

5. E.V. Pereloma: *Mater. Sci. Technol.*, 2016, vol. 32, pp. 99-103.
6. C. Garcia-Mateo, J. Jimenez, H.W. Yen, M.K. Miller, L. Morales-Rivas, M. Kuntz, S. Ringer, J.R. Yang, and F.G. Caballero: *Acta Mater.*, 2015, vol. 91, pp. 162-173.
7. Z.P. Xiong, A.A. Saleh, R.K.W. Marceau, A.S. Taylor, N.E. Stanford, A.G. Kostryzhev, and E.V. Pereloma: *Acta Mater.*, 2017, vol. 134, pp. 1-15.
8. F.G. Caballero, H.W. Yen, M.K. Miller, J.R. Yang, J. Cornide, and C. Garcia-Mateo: *Acta Mater.*, 2011, vol. 59, pp. 6117-6123.
9. E.V. Pereloma, I.B. Timokhina, M.K. Miller, and P.D. Hodgson: *Acta Mater.*, 2007, vol. 55, pp. 2587-2598.
10. W. L. Fink and E. D. Campbell, Trans. Am. Soc. Steel Treat. 1926, vol. 9, pp.717-52.
11. N. Seljakow, J. Kurdumoff and N. Goodtzov, Nature, 1927, vol.119, p. 494.
12. K. Honda, Z. Nishiyama, Sci. Rpts. Tohoku. Imp. Univ. Ser. 1, 1932, vol. 21, p. 299.
13. M. Cohen, *Trans. Metall. Soc. AIME*, 1962, vol. 224, pp. 638-54.
14. Z. Fan, L. Xiao, Z. Jinxiu, K. Mokuang and G. Zhenqi, Phys. Rev. B, 1995, vol. 52 (14), pp. 9979-87.
15. H.K.D.H. Bhadeshia: *Philos. Mag.*, 2013, vol. 93, pp. 3714-3725.
16. C. Hulme-Smith, I. Lonardelli, A. Dippel, and H.K.D.H. Bhadeshia: *Scripta Mater.*, 2013, vol. 69, pp. 409-412.
17. C.N. Hulme-Smith, M.J. Peet, I. Lonardelli, A. Dippel, and H.K.D.H. Bhadeshia: *Mater. Sci. Technol.*, 2015, vol. 31, pp. 254-256.
18. Z.P. Xiong, A.G. Kostryzhev, A.A. Saleh, L. Chen, and E.V. Pereloma: *Mater. Sci. Eng. A*, 2016, vol. 664, pp. 26-42.
19. D.R. Mitchell and J. Van den Berg: *Ultramicroscopy*, 2016, vol. 160, pp. 140-145.
20. E.V. Pereloma, H. Beladi, L. Zhang, and I.B. Timokhina: *Metall. Mater. Trans. A*, 2012, vol. 43, pp. 3958-3971.
21. S. Morito, J. Nishikawa, and T. Maki: *ISIJ Int.*, 2003, vol. 43, pp. 1475-1477. 22. J. Fisher: *JOM*, 1949, vol. 185, pp. 688-690.
23. C. Roberts: *J. Met.* 1953, vol. 197, pp. 203-204.
24. Y. Lu, H. Yu, and R.D. Sisson Jr: *Mater. Sci. Engi. A*, 2017, vol. 700, pp. 592-597. 25. L. Kremnev: *Tech. Phys.*, 2013, vol. 58, pp. 1288-1290.